frontiers | Frontiers in Marine Science

TYPE Original Research
PUBLISHED 12 May 2023
DOI 10.3389/fmars.2023.1165551

OPEN ACCESS

EDITED BY
Nicoletta Leonardi,
University of Liverpool, United Kingdom

REVIEWED BY
Pedro Cunha,
University of Coimbra, Portugal
Shuhuan Du,
South China Sea Institute of Oceanology (CAS), China
Morthekai Paulramasamy,
Birbal Sahni Institute of Palaeosciences (BSIP), India

*CORRESPONDENCE
Yang Yang
yyang@njnu.edu.cn
Gaocong Li
gcli@gdou.edu.cn

RECEIVED 14 February 2023
ACCEPTED 21 April 2023
PUBLISHED 12 May 2023

CITATION
Zhou L, Yang Y, Li G and Tong C (2023) OSL dating of coastal dunes on the southeastern coast of Hainan Island, China. *Front. Mar. Sci.* 10:1165551. doi: 10.3389/fmars.2023.1165551

OSL dating of coastal dunes on the southeastern coast of Hainan Island, China

Liang Zhou[1,2], Yang Yang[3,4]*, Gaocong Li[1,5]* and Changliang Tong[1]

[1]Hainan Key Laboratory of Marine Geological Resources and Environment, Hainan Marine Geological Survey Bureau, Haikou, China, [2]School of Geography, Geomatics, and Planning, Jiangsu Normal University, Xuzhou, China, [3]Ministry of Education Key Laboratory for Coast and Island Development, Nanjing University, Nanjing, China, [4]School of Marine Science and Engineering, School of Geography, Nanjing Normal University, Nanjing, China, [5]Department of Marine Technology, Guangdong Ocean University, Zhanjiang, China

Coastal dune sediments and landforms offer a unique opportunity to understand climate change and sea level change on the centennial-millennial time scale. However, there is a paucity of chronological studies on the effects of storms on the evolution of coastal dunes along the temperate coastline of China. In this study, optically stimulated luminescence (OSL) dating of sand dunes was conducted to investigate the process and mechanism of coastal dune evolution on the southeastern coast of Hainan Island, China. The results show that the coastal dune evolution experienced three rapid accumulation periods: 28-21 ka, 14-4 ka, and 3.0 ka-present. The three rapid accumulation periods correspond to the last glacial maximum, the late Pleistocene/early-mid Holocene, and the late Holocene climatic dry-cold period, respectively. Sea level change and the East Asian winter monsoon, in conjunction with the enhanced storminess, play a key role in driving the sand dune evolution on the south-eastern coast of Hainan Island. These findings are of great significance for regional planning and coastal defense schemes.

KEYWORDS

palaestorm events, southeastern Hainan Island, OSL dating, East Asian winter monsoon, coastal dune

1 Introduction

Coastal dunes, which lie between marine and land areas, often play an important role protecting humans against natural hazards (e.g. storm events; Dissanayake et al., 2015; Martinez et al., 2016; Maximiliano-Cordova et al., 2021). With global warming, coastal dunes are facing the ongoing threats of sea level rise, climate change, and changes in storm intensity (Defeo et al., 2009; Morris et al., 2020). The knowledge of past coastal dune evolution is critical for forecasting trends of sea level rise and coastal storm disaster management practices. Coastal dune deposits have the great potential to provide records of coastal processes, storm activities, environmental changes, and sea level fluctuations (Kunz

et al., 2010; Wolfe et al., 2011; Clemmensen et al., 2012; Clemmensen et al., 2014; Zhou et al., 2019a).

Based on coastal dune deposits, reconstruction of paleoenvironment change and sea level changes have been studied in various coastal areas including those in southeastern Australia (Ashkenazy et al., 2012; Tamura et al., 2020), America (Wolfe et al., 2011; Robin et al., 2021), Denmark (Clemmensen et al., 2012; Clemmensen et al., 2014), the Mediterranean (Zazo et al., 2008; Bardají et al., 2009), Japan (Tamura et al., 2011a, b), and South China (Jin et al., 2022). These findings improved our understanding of past changes in atmospheric circulation and sea level changes (Searle and Woods, 1986; Tamura et al., 2011a; Tamura et al., 2011b; Clemmensen et al., 2014; Hu et al., 2022; Jin et al., 2022). However, there are few such studies of the effects of storms on coastal dune evolution in the tropical coastal zone, especially on the South China Coast (e.g. Hainan Island, Li et al., 2007).

The chronology of coastal dunes is a significant issue for the temporal analysis of coastal dune evolution and the interpretation of these variable responses to climate changes and storm behavior. The main methods for dating palaestorm events from coastal dunes are luminescence dating of the sand and radiocarbon dating of organic material or marine shells (Murray and Clemmensen, 2001; Sommerville et al., 2003; Cunningham et al., 2011; Clemmensen et al., 2014; Zhou et al., 2019a). Radiocarbon dating has limited applicability owing to the lacking of organic material in these coastal dune sediments and overwash deposits. Moreover, if shells exist, they are commonly contained within lagoonal or shelf sediments and are not part of the barrier lithosome. However, optical luminescence techniques proved capable of establishing an absolute chronology for coastal sediments in various coastal environments (van Heteren et al., 2000; Sommerville et al., 2003; Reimann et al., 2012; Chazan et al., 2013; Jiang et al., 2018; Gao et al., 2019; Zhou et al., 2019a; Nian et al., 2021).

The coastal dune in southeastern Hainan Island was selected in this study. The coastal dune in this region has been frequently and seriously affected by tropical storms from the northwestern Pacific and South China Sea (SCS). We present the measured OSL ages from 6 profiles at two sites in the area and compared them with previous chronology and historical records in southeastern Hainan Island, to reconstruct the history of the coastal dune evolution, and to reveal the effect of storm activities on dune evolution.

2 Study areas

Hainan Island is separated from the Chinese mainland by the narrow Qiongzhou Strait (Figure 1). The island has a staircase-like topography, descending step by step from towering mountains to flat tablelands and plains at its periphery. This island covers an area of 33900 km^2 with a coastline of 1725 km in length (Song, 1984). The oceanographic conditions on its southeastern coast are characterized by micro-tides, irregularly diurnal in character. Here, the climate for the coastal region is generally tropical monsoonal, with a dry season from November to April and a wet season from May to October. Typhoons and tropical cyclones from the western Pacific Ocean and the SCS frequently hit the southeastern coast of Hainan Island from July to October (Wang et al., 2001). During typhoon events, the accompanying high wind speeds, large storm surges, and waves often cause serious damage to the coastal infrastructure and residential areas.

The Li´an (LA) dune is about 5 km long and 1 km wide, located on the east side of the Li´an Lagoon. The longshore transport of sand, generated by the prevailing shore currents from the NNE, is constrained by the southerly headland. The LA dune experiences a micro-tidal regime with an average tidal range of 0.65 m and a maximum tidal range of 1.50 m, as measured in the Li´an Lagoon (Wang et al., 2016). Waves approach from the SEE (South-East-East) for (on average) 90% of the year, and from the ESE (East-South-East) during the remaining 10% of the time. Wave height ranges from 0.30 m to 1.8 m, with rare exceptional heights of more than 3.7 m. Such high waves are associated with storms from the SW, during which waves attain an average of 2–3 m height with a period of 7–8s.

The Jianling (JL) dune, located on the southeast side of Xincun Lagoon, both sides are bound by low hills. The beachfront is surrounded by a coral reef and bedrock platform (20-50 meters wide). Behind the beach, there is a large area of coastal dune with a top elevation of more than 15 msl.

3 Material and methods

3.1 Sampling and preparation

Sediment samples were collected between 2015 and 2016 from the Li′an (LA) site and Jianling (JL)site (Figures 2, 3). During fieldwork, three profiles (LA-A, LA-E, and LA-M) along fresh ditches at the LA site and three exposure profiles (JL-A, JL-B, and JL-C) at the JL site (Figures 2, 3), were observed and pedo-stratigraphically described in detail. Pedostratigraphic subdivisions were observed by close examination of the color, texture, and structure in these profiles (Figures 2, 3). Storm deposits were distinguished in the field using sedimentological criteria (e.g. numerous planar beds; abrupt contracts; Zhou et al., 2019a). Several typical samples were taken from each profile for grain size analysis. Particle-size distribution was analyzed using a Malvern Mastersize 2000 laser granulometer with a duplicate measurement error of < 3%. Statistical indices such as median (Md), mean (Mz), skewness (Sk), kurtosis (Kg), and sorting (QD) were calculated using the GRADISTAT program (Blott and Pye, 2001).

3.2 Luminescence dating

Eight OSL samples were collected by hammering steel tubes into cleaned profile walls. We first used 10% HCl and 30% H_2O_2 to remove any carbonates and organic material in the OSL samples, before wet sieving to obtain the 90-125 μm fraction. The sand grain fraction was etched by a 40% HF for about 40 minutes to remove any feldspar and the surfaces of the grains, and then a final 10% HCl wash to remove any fluorides which may have formed during the HF treatment (Lang et al., 1996; Chamberlain et al., 2017; Zhou

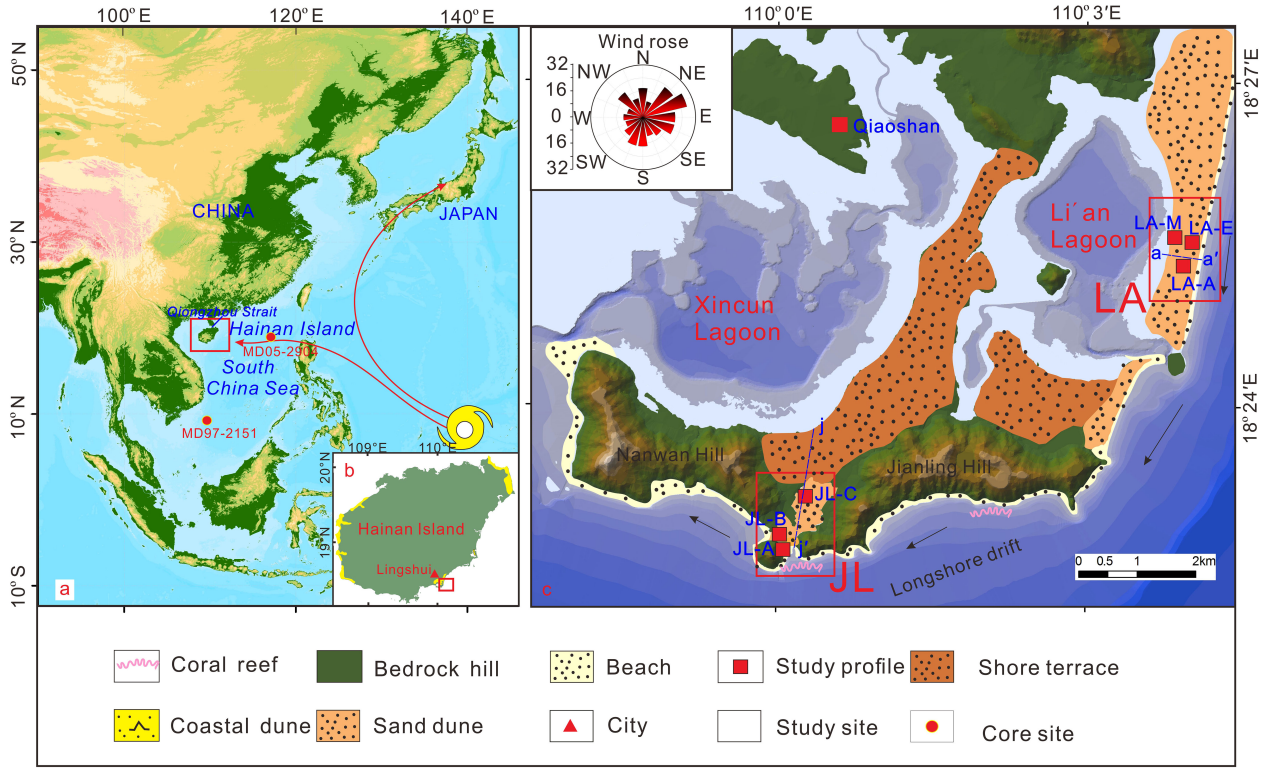

FIGURE 1
The study area in the SCS. **(A)** and Hainan Island **(B)**, and the location of study of the study sites **(C)**.

et al., 2019a; Guo et al., 2023). We carried out an IR test to make sure the samples were pure enough. OSL samples *De* measurements were carried out on small aliquots (200-400 grains per aliquot). Luminescence measurements were undertaken on an automated Riso TL/OSL system (TL-DA-15) equipped with blue LEDs (470 ± 30 nm) for stimulation. We used the OSL signal from the first 0.8 s of stimulation and subtracted the background signal estimated from the integral of the last 4 s of stimulation. The single aliquot regenerative procedures (Murray and Wintle, 2003) were used for the equivalent dose (*De*) determination.

The environmental dose rates were derived from measured radioactive element concentrations (Adamiec and Aitken, 1998). The contents of U, Th, and K in the OSL samples were determined by neutron-activation-analysis (NAA) at the China Institute of Atomic Energy (Zhang et al., 2012). The water content was estimated with an uncertainty of ±5%. The effective dose rate was calculated by an AGE program (Grün, 2009).

3.3 RTK elevation measurement

The RTK–DGPS survey system was used to obtain high-accuracy elevation and positional data for the profile. The RTK system has an accuracy of ±10 mm for elevation measurements. In order to obtain the elevation with reference to the local datum, reference points were used. We also conducted a-a′ and J-J′ transect (Figure 1C) at 20–80 m intervals across the LA dune and JL dune, respectively.

4 Results and discussion

4.1 OSL ages

Typical natural OSL decay curves and dose–response curves for coarse-grained quartz fractions from samples LA-A-01 and JL-B-01 are shown in Figure 4. The OSL signals rapidly decay to near-background levels, implying that OSL signals from the two OSL samples are dominated by the fast component. The consistency of the first regeneration dose point and its repeated dose points suggests that the sensitivity changes during OSL measurements were corrected appropriately. The OSL signals produced by zero doses are close to zero, suggesting that thermal transfers during measurement are negligible.

A preheat plateau experiment was carried out on OSL samples LA-A-01 and JL-B-01, with preheat temperatures increasing from 180°C to 280°C at 20°C intervals. At least three aliquots were measured using the SAR protocol at each temperature. For sample LA-A-01, the result shows that there is a plateau of De values on preheat temperatures from 200 to 260°C (Figure 5A). Thermal transfer varies in the range of -0.02–0.17 Gy (JL-B-01) and 0.03-0.22 Gy (LA-A-01) between 180°C and 280°C, respectively. The thermal transfer from the 0 Gy regenerative dose for JL-B-01 and LA-A-01 range from 0-1.9% and 0.5%-3.3% (Figure 5A), respectively. This indicates that thermal transfer can be negligible for LA-A-01. A dose recovery test using blue LEDs was also performed on the same samples LA-A-01 and JL-B-01, to further

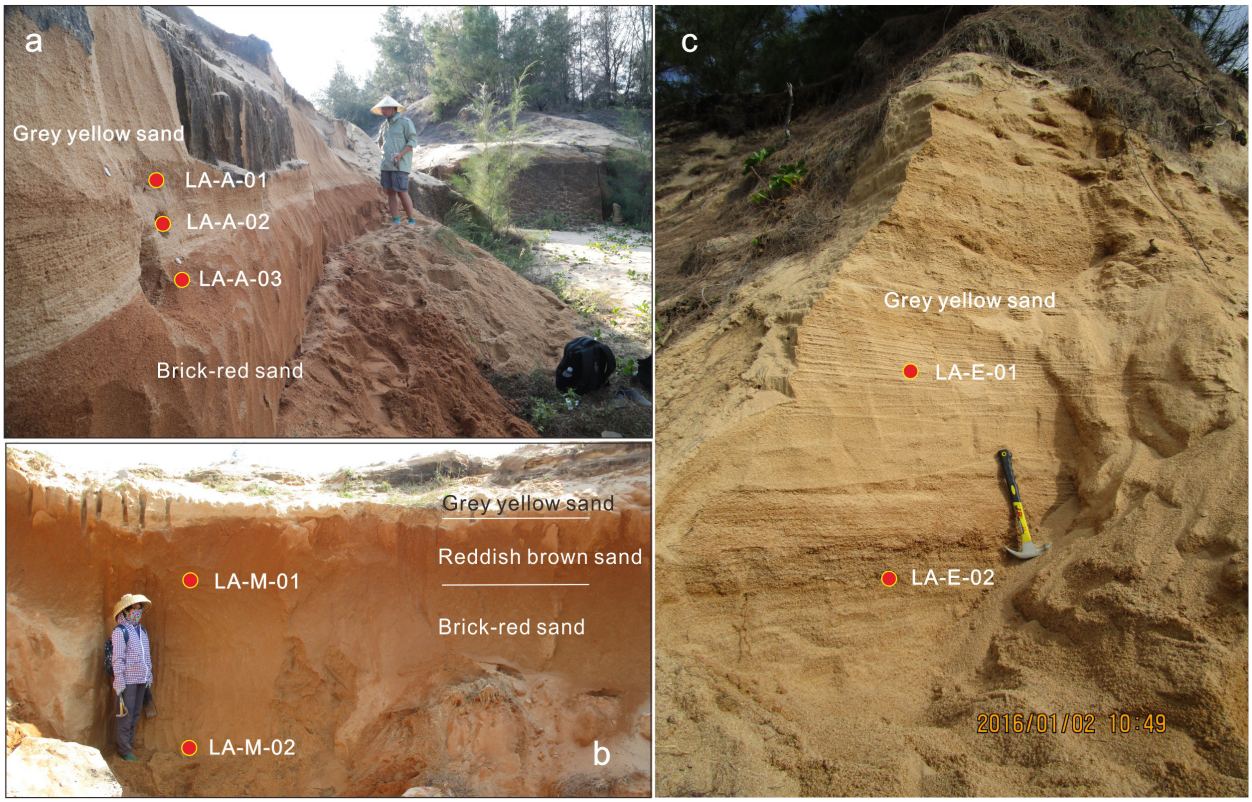

FIGURE 2
Photographs of the studied profiles LA-A**(A)**, LA-M**(B)**, LA-E**(C)** at the LA site along southeastern Hainan Island. Red circles denote the OSL samples.

validate the SAR procedure for these samples. The given doses for samples LA-A-01 and JL-B-01 are 6.86 Gy and 0.92 Gy, respectively. The recovery ratios (measured dose/given dose) obtained for each aliquot as a function of preheat temperature (Figure 5B) show that the measured doses are statistically consistent with the given doses in the preheat temperature range of 200–260°C. Furthermore, the recycling ratios at 200°C (for OSL sample LA-E-01) and 220°C (for OSL sample LA-A-01) display the smallest scatter between aliquots. To minimize the effects of the thermal transfer of young samples, therefore, a preheat temperature of 200°C was chosen for the OSL sample in JL-A and JL-B, and 220°C was chosen for the OSL sample in LA-A, LA-E, LA-M, and JL-C profiles for De determination of all the samples.

Table 1 shows all the samples have relatively high OD values (OD>20%), implying that sediments at the two sites have experienced insufficient bleaching. To minimize the effects of partial bleaching, a formal decision procedure (Galbraith et al., 1999; Zhang et al., 2019) was used to determine all OSL sample ages, as indicated in Arnold et al. (2007). The results show that no chronological inversion occurred in all ages (Table 1). Environmental archaeological investigations have been conducted in this area (Fu et al., 2016), and the archaeological age provides the possibility of stratigraphic correlation. In the adjacent Qiaoshan site, the Neolithic culture layer interbedded between the grey-yellow sand layer and the reddish-brown sand layer, yield the age of 3.0-3.50 ka (Fu et al., 2016). In the LA-A and LA-E, the OSL samples collected from the bottom of the grey-yellow sand layer (LA-A-01 and LA-E-02), were dated to 3.0 ± 0.1 ka and 0.31 ± 0.20 ka, respectively. The OSL results and archaeological age from the two sites are remarkably consistent. In addition, the OSL age of JL-C-01 from the top of Brownish red sandy soil layer was OSL dated to 4.02 ± 0.26 ka, which is very close to its underlying culture layer age (Lianzi Bay Culture; ~5 ka; Fu et al., 2016; Table 1; Figures 3D, 6). Therefore, our OSL ages in this study are reliable.

By plotting all OSL dates from the two sites, we can conclude that the coastal dunefield in the LA-A site mainly formed in the episode of >28-21 ka, 21-8 ka, and since 3.1 ka (Figure 6), and the coastal dunefield in the JL site mainly formed in the period of 14.1-4.0 ka, 4.0-0.3 ka, and 0.3-0.1 ka (Figure 6). The lithostratigraphy and the OSL ages obtained in the two sites can be integrated to provide the aggradation ages of the lithostratigraphic sand units: Yellow-brown sand as >28 to 21 ka; Brownish-red sand and brownish-yellow sand as 14 to 4 ka; Grey-yellow sand, grey sand, and storm deposits as comprising the last 3 ka.

4.2 Grain size

The grain-size fractions and the statistical indices of the sediments from the LA site and JL site are listed in Table 2. The non-storm deposit in the LA site is dominated by coarse sand (18.47%-29.41%) and very coarse sand (23.49%-69.07%). Storm

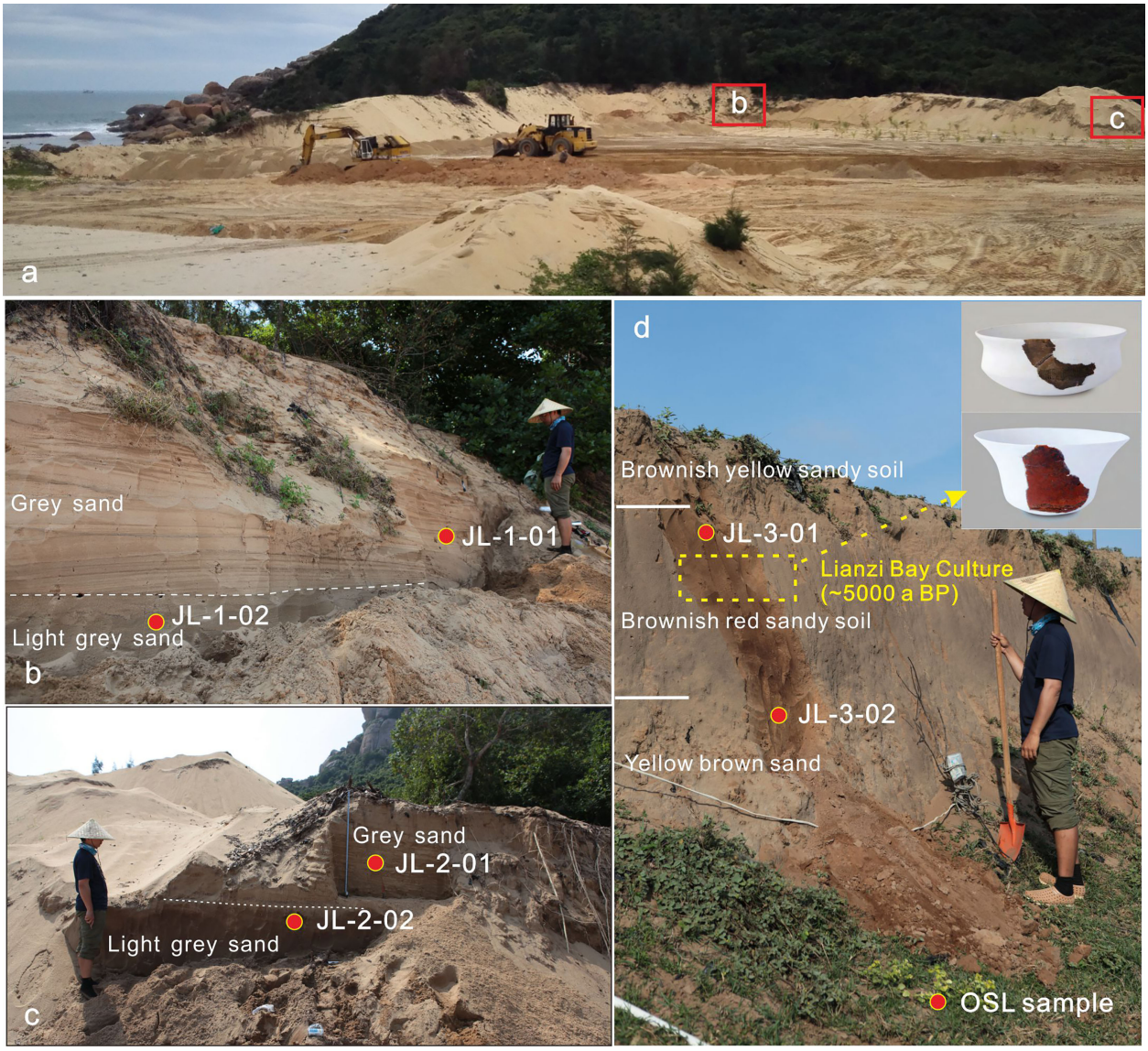

FIGURE 3
(A) the location of JL-1 and JL-2 profiles. **(B-D)** Photographs of the studied profiles (JL-1, JL-2, JL-3) at the JL site.

deposits from the LA-A and LA-E profiles are dominated by very coarse sand (68.11%-75.14%), with a mean of 637.25 μm -646.18 μm, respectively. Non-storm deposits in the JL site are dominated by fine sand (24.15%-30.31%) and medium sand (49.54%-63.12%) and mean grain sizes range from 266.57 μm to 364.77 μm. Storm deposits from the JL-A profile are dominated by very coarse sand (82.88%), with a mean of 833.83 μm.

4.3 Coastal dunes evolution on the southeastern Hainan coast

4.3.1 Stratigraphy and chronology

LA-A site, the upper grey-yellow sand unit, and the lower brick-red sand unit were separated by erosional unconformity storm deposits (Figure 2A; Zhou et al., 2019a). The lower unit is dominated by coarse sand and poorly sorted, weakly weathered or pedogenically modified, scattered fine gravel. The upper unit exhibits a similar sedimentary structure and comprises loose coarse, poor-sorted, with few scattered granules and gravel. The OSL samples LA-A-01and LA-A-02 sampled from the bottom of this unit were dated to 2.80 ± 0.20 ka and 2.96 ± 0.10 ka (Figure 2A; Table 1), respectively, which means the dune sediment in the LA site has been mainly deposited since around 3 ka.

LA-E site, a medium and coarse sand grey yellow sand behind the LA Beach, displays a weakly developed, loose, and structureless texture. This profile interbedded with some slightly laminated and moderately parallel bedding, indicating these layers deposition under storm events (Zhou et al., 2019). An OSL sample collected from the bottom of the profile was dated to 3.10 ± 0.18 ka (Figure 2C; Table 1), suggesting dune deposition also mainly occurred over the last 3.0 ka.

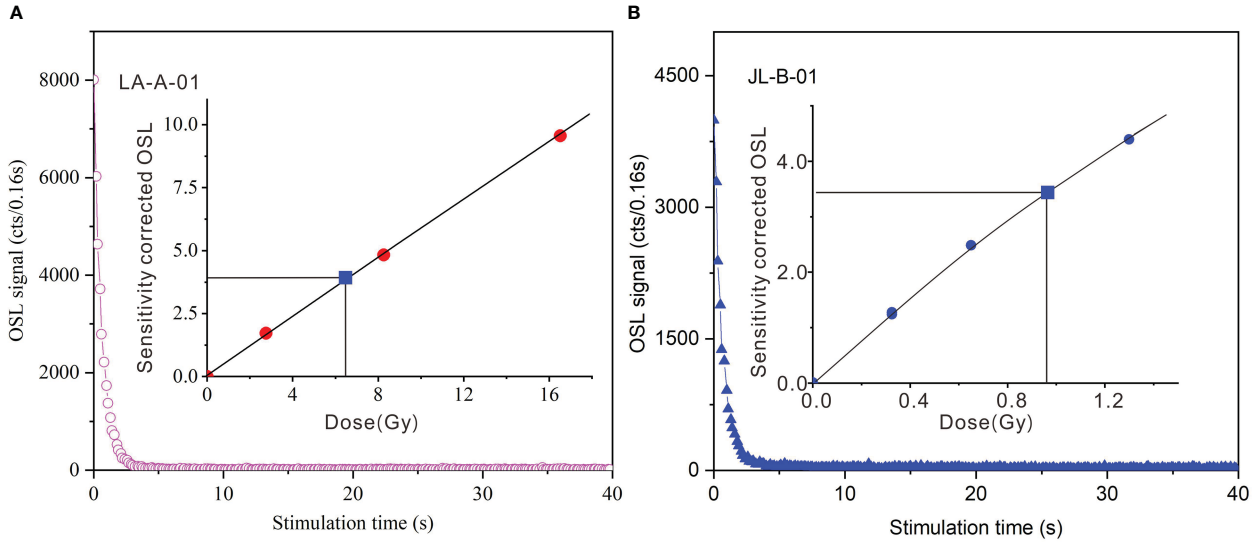

FIGURE 4
Luminescence properties of samples LA-A-01 and JL-B-01. Natural OSL decay curves for coarse-grained quartz **(A, B)**. Insets are growth curves obtained using the SAR protocol (see the text) for the same aliquots as the decay curves. Filled squares represent sensitivity-corrected natural OSL signals.

LA-M site, this 3.8 m road cutting reveals three sedimentary units. The upper grey-yellow sand unit was similar to the LA-E site. The reddish-brown middle unit consists of coarse-grained quartz sand, with no discernable bedding or changes in texture. The base of this profile, is composed of brick-red coarse sand, weakly weathered, loose, and structureless in texture. The LA-M-02 sampled from the bottom of this profile were dated to 27.60 ± 2.50 ka. The lower layer of reddish-brown sand was OSL dated to 7.59 ± 0.90 ka (LA-M-01; Table 1). In addition, the OSL sample LA-A-03 collected from the top of the brick-red sand unit was dated to 20.85 ± 2.40 ka. This means that the brick-red sand unit in the LA-M site was mainly deposited between 28 ka and 21ka.

JL-A profile is about 220 m from the shoreline, and the base of the profile consists of gray-black sandy soil with much moisture. Overlying this bottom layer are storm overwash deposits with typical parallel bedding characteristics (340 cm). The JL-B profile is

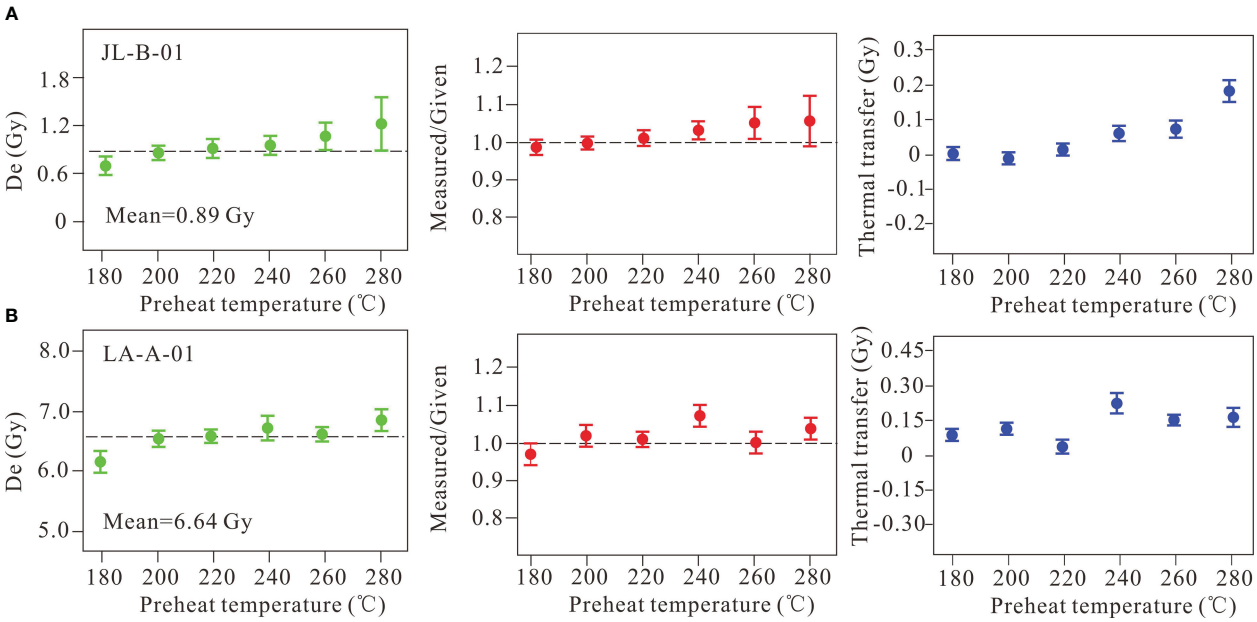

FIGURE 5
(A) Plots of equivalent dose, measured/given, and thermal transfer versus preheat temperature for coarse-grained quartz of sample JL-B-01. **(B)** Plots of equivalent dose, measured/given and thermal transfer versus preheat temperature for coarse-grained quartz of sample LA-A-01.0.0780.94.

10.3389/fmars.2023.1165551

TABLE 1 OSL ages from LA and JL site, southeastern Hainan Island (LA-A and LA-E source from Zhou et al., 2019a).

Sample	Depth (m)	De (Gy)	OD (%)	Water content (%)	U (ppm)	Th (ppm)	K (%)	Dose rate (Gy/ka)	Model	Age (ka)
LA-A-01	1.77	6.34 ± 0.26	32	15	1.42 ± 0.07	4.21 ± 0.01	1.79 ± 0.04	2.24 ± 0.11	MAM	2.80 ± 0.20
LA-A-02	1.97	7.14 ± 0.53	46	12	1.45 ± 0.07	4.82 ± 0.01	1.83 ± 0.05	2.41 ± 0.13	MAM	2.96 ± 0.10
LA-A-03	2.23	34.95 ± 3.87	35	20	0.96 ± 0.06	4.20 ± 0.01	1.27 ± 0.03	1.68 ± 0.05	MAM	20.85 ± 2.40
LA-E-01	3.73	5.78 ± 0.28	30	12	1.12 ± 0.05	2.98 ± 0.01	1.41 ± 0.02	1.86 ± 0.20	MAM	3.10 ± 0.20
LA-E-02	2.43	2.09 ± 0.18	50	15	1.28 ± 0.04	4.76 ± 0.02	1.53 ± 0.02	2.10 ± 0.10	MAM	1.04 ± 0.05
LA-M-01	1.74	21.59 ± 3.19	45	15	1.51 ± 0.07	5.90 ± 0.02	1.92 ± 0.05	2.45 ± 0.07	MAM	7.59 ± 0.90
LA-M-02	3.53	37.07 ± 3.15	43	12	0.83 ± 0.06	3.22 ± 0.12	0.99 ± 0.04	1.34 ± 0.04	MAM	27.60 ± 2.50
JL-A-01	1.15	0.19 ± 0.10	65	12	1.63 ± 0.08	8.55 ± 0.26	0.97 ± 0.04	1.42 ± 0.04	MAM	0.13 ± 0.03
JL-A-02	1.73	0.79 ± 0.17	36	15	5.01 ± 0.15	34.0 ± 0.78	1.12 ± 0.04	4.13 ± 0.10	MAM	0.19 ± 0.02
JL-B-01	1.10	0.40 ± 0.05	47	15	1.63 ± 0.08	8.55 ± 0.26	0.97 ± 0.04	1.88 ± 0.06	MAM	0.21 ± 0.03
JL-B-02	2.32	0.38 ± 0.06	34	15	1.20 ± 0.07	3.86 ± 0.14	0.813 ± 0.03	1.35 ± 0.04	MAM	0.28 ± 0.05
JL-C-01	0.75	5.98 ± 0.30	22	15	1.43 ± 0.07	7.83 ± 0.25	0.58 ± 0.03	1.47 ± 0.04	CAM	4.12 ± 0.24
JL-C-02	2.35	21.48 ± 3.21	25	18	2.54 ± 0.10	7.90 ± 0.25	0.475 ± 0.02	1.53 ± 0.04	MAM	14.08 ± 2.14

about 300 m away from the shoreline, and the storm deposits occur at the top of the coastal dunes with a thickness of about 2~3 m; the dunes are characterized by obvious stratification, parallel bedding structure. The bottom sediment of this profile was gray-black sandy soil. The JL-A-02 and JL-B-02 collected from the bottom of JL-A and JL-B profiles was OSL dated to 0.19 ± 0.02 ka and 0.28 ± 0.05 ka, respectively (Figures 3, 6; Table 1). This means the sand dune at the JL-A site was mainly formed over the past 0.3 ka.

The JL-C profile was about 1200 m from the sea and can be divided into three parts. The lower part was yellow-brownish sand

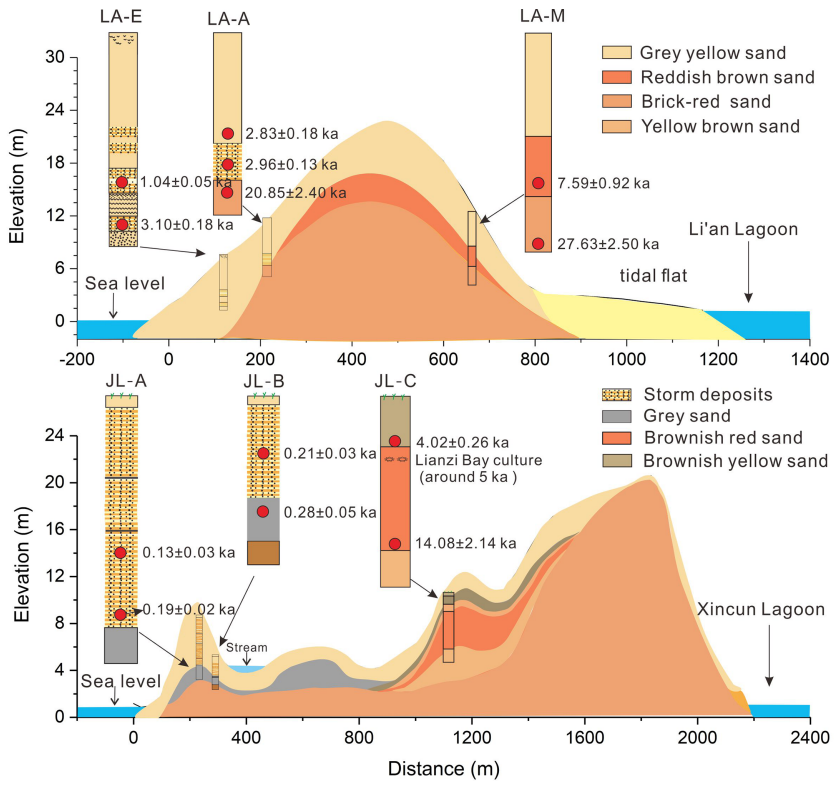

FIGURE 6
A generalized, schematic cross-section through the dune field at the LA and JL sites showing major stratigraphic features and the OSL ages.

10.3389/fmars.2023.1165551

TABLE 2 Grain size data for the sediments in the LA site and JL site.

Profile	Sample layer	Mean (μm)	*S*	*Kg*	*SK*	<63 μm (%)	63-250 μm (%)	250-500 μm (%)	>500 μm (%)
LA-a	Grey yellow sand	353.13	1.36	2.28	1.25	7.71	21.26	32.01	39.01
	Storm deposits	637.25	1.29	1.27	1.54	20.29	4.14	7.46	68.11
	Brick red sand	482.97	1.41	1.92	1.34	6.69	10.73	28.84	53.47
LA-E	Grey yellow sand	486.33	1.54	2.34	1.77	4.70	11.45	27.67	56.18
	Storm deposits	646.18	1.60	1.87	2.07	9.78	2.71	12.37	75.14
LA-M	Grey yellow sand	425.47	1.92	2.42	1.16	12.54	6.73	29.41	51.20
	Reddish brown sand	547.93	1.23	2.57	0.98	5.74	6.18	20.03	68.05
	Brick red sand	582.97	1.51	1.74	1.22	4.77	7.69	18.47	69.07
JL-A	Yellowish grey sand	353.51	0.68	0.99	0.09	0.00	24.15	52.36	23.49
	Storm deposits	833.83	0.82	1.22	0.27	2.20	4.09	11.02	82.88
	Grey sand	266.57	1.38	3.08	-0.44	12.29	28.19	52.69	7.46
JL-B	Yellowish grey sand	319.72	0.68	1.01	0.08	1.05	29.83	51.69	17.43
	Grey sand	289.65	1.14	2.26	-0.32	7.85	28.95	50.34	12.86
JL-C	Brownish yellow sandy soil	281.51	1.35	2.65	-0.41	11.59	27.67	51.92	8.82
	Brownish red sandy soil	278.46	1.79	2.88	-0.53	14.57	30.31	49.54	5.58
	Yellow brown sand	364.77	1.46	2.13	-0.38	3.43	24.96	63.12	8.49

S, sorting; Kg, kurtosis; SK, skewness.

(below 250 cm), the middle unit was brownish-red sandy soil (250-75cm), and the upper unit was brownish-yellow sandy soil (0-75cm). JL-C-02 collected from the top of the middle unit was OSL dated to 4.12 ± 0.24 ka (Figures 3, 6; Table 1). The JL-C-01 collected from the bottom of the lower unit (yellow-brownish sand) was OSL dated to 14.08 ± 2.14 ka (Figures 3, 6; Table 1). This means that the dune at the JL-C site was mainly formed between 14 ka and 4 ka.

4.3.2 The role of sea level rise and climate change on the coastal dune formation

Previous studies show that coastal dune formation has been linked to sea-level change (Tamura et al., 2011b; Zazo et al., 2008), sand supply (Zheng et al., 2021), and climate change (Aagaard et al., 2007; Hu et al., 2022). According to the dating results from the LA site and JL site, the dune sediment mainly accumulated in periods of >28-21 ka, 14-4 ka, and the last 3 ka (Figure 7E; *Section* 4.3.1). Comparison of the three age periods with previous studies on Hainan Island (Figure 7E) displayed the dune formation period generally overlaps the periods of coastal dune development in Hainan Island.

Figures 7C, E shows that the timing of the first dune formation period (>28 - 21 ka) was apparently synchronous with the sea-level depression period and the last glacial maximum (LGM) episode. During the LGM period, the sea level of the north part of the SCS dropped 150-200 m (Wu and Wang, 1997). The continental shelf in the north part of the SCS (e.g. the continental shelf around Hainan Island) was exposed as an inland area, which provides an abundant aeolian sand source for the development of sand dunes. In addition, the strong northeast winter wind owing to the stronger winter monsoon (Figure 7D) provided a powerful driving force to transport the rich sand sediment from the shelf to the coastal land. Therefore, the accumulation of dune sands in the P1 period has been associated with extremely dry and cold weather and significant sea-level drop during the LGM period.

The timing of the second dune formation period (14-4 ka) falls into the late Pleistocene/early-mid Holocene period. Figure 7C, E, this episode corresponds to the period of rapid sea level rise period. Previous studies have evidenced that rapid accumulation of coastal dune sediment could occur in the period of the sea-level highstands (Murray-Wallace et al., 2010; Tamura et al., 2011b; Zheng et al., 2021). Because a warm and humid climate greatly increases soil weathering and erosion, more sediment was delivered into the shore areas by rivers during the sea-level rises, which provide sufficient sources for coastal dune activities (Tamura et al., 2011b). However, Zheng et al. (2021) indicated that coastal dune sand records of Hainan Island in the early-mid Holocene were not continuous, indicating that other factors (e.g. winter monsoon) may play an important role in affecting coastal dune sand accumulation during the second dune formation period. A comparison of Figures 7D, E shows that the second dune formation period is generally in a strong winter monsoon stage, although the winter monsoon intensity is not as strong in the SCS as it is in the LGM period. The northward of ITCZ (Figure 7B) in the period may strengthen the intensity of the winter monsoon. The sand source of this second period is the near-source sands transported by winter onshore

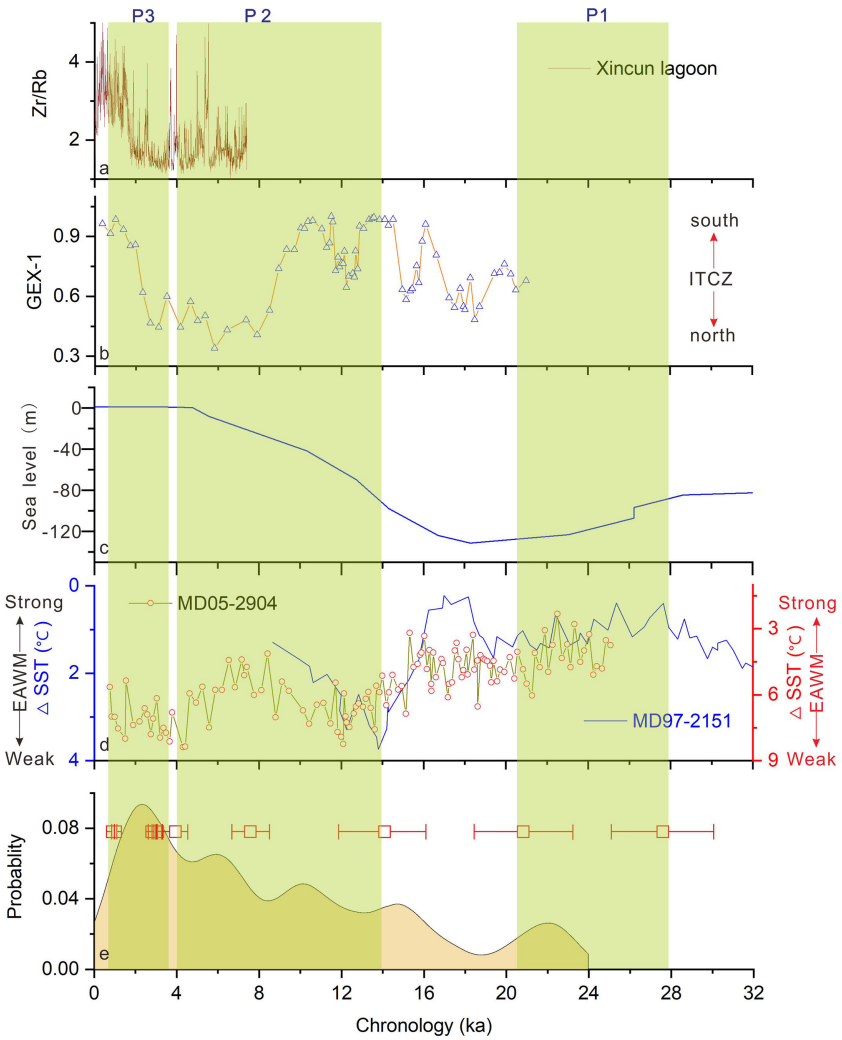

FIGURE 7
Comparison of the Age distribution of samples at the Hainan Island sites with paleoclimatic, sea level change proxies. **(A)** The storm records from Xincun Lagoon in southeastern Hainan Island; **(B)** late Quaternary ITCZ proxy from the Cariaco Basin (Mertens et al., 2009); **(C)** Relative Sea level derived from benthic foraminifera isotopic records (Waelbroeck et al., 2002); **(D)** winter monsoon variations recorded by the core MD05-2904 and MD97-2151 in the northern SCS (Steinke et al., 2011; Yamamoto et al., 2013); **(E)** frequency of dune formation period at the Hainan Island based on the kernel density estimate of ages of dune deposits. The age bar represents the dune age data from this study.

winds, in addition to tides and waves. Similar active dune activities have been widely evidenced in areas at the same latitude (e.g. India, Vietnam; Colin et al., 2002; Alappat et al., 2013; Tamura et al., 2020). Therefore, the accumulation of dune sands in the P2 period is possibility associated with the relatively stronger winter monsoon. The color of the sand in this period was the deepest color, which should be related to the warm and humid climate in this episode.

The dune formation in the P3 period (3.0 ka-present) coincided with the late Holocene climate deterioration phase. This period features a decreasing temperature, weakening summer winds, and a decrease in humidity (Zhao et al., 2009), which reinforces the winter wind forces. In addition, geochemical records from the continental shelf of Hainan Island indicated human activities have greatly increased since 4.0 ka (Xu et al., 2018). The increased human activities could bring abundant sediments to the coast from the river basin. Under the action of a dry climate, intensified EAWM (East Asian winter monsoon), and increased human activities, the coastal dune was well developed along the coast of Hainan Island over the past 3 ka (Figure 7E). Interestingly, coastal sand dune activities were also significantly strengthened along the coast of South China (Zheng et al., 2021), Japan (Tamura et al., 2016), and Korea (Kunz et al., 2010) during the late Holocene.

4.3.4 The role of storm events in the southeastern coastal dune formation

It's worth noting that the later stage of the third period corresponds well to the period of intensified storm activity (Figures 7A, E). In addition, huge storm deposits have accumulated in the JL-A site over the past 300 years (Figure 6), suggesting that storm activities may be responsible for the building of the coastal dunes at southeastern Hainan Island. Previous studies indicated that storm activities have been an important factor that

influences coastal dune sediment accumulations in South China (Hu et al., 2022), Australia (Tamura et al., 2018), and North America (Harris and Ellis, 2021). In Hainan Island, sediment records and historical documents show that storms have frequently hit southeastern Hainan Island over the past few thousand years (Zhou et al., 2019a; Zhou et al., 2019b), which are not only generated from the western Pacific but also from the SCS. However, there is a lack of understanding of the process and mechanism of storms on the building of coastal dunes on Hainan Island.

The aeolian deposits at the LA site were dominated by coarse sand and very coarse sand, with a mean grain size at about 260–830 μm (Table 2). A small amount of gravel was also identified in the dune deposits at the LA site (*Section* 4.2.1). Winter winds are believed to be the primary factors responsible for the formation of the coastal dune along Hainan Island (Zheng et al., 2021). However, the winter wind does not normally have the ability to transport a large amount of coarse sand to the top of the sand dune, because of the weak power of non-storm winds on the coast of eastern Hainan Island (Wu and Wu, 1995). Studies have shown that storm winds (>27 m/s) and even non-storm winds are capable of transporting coarse sand (Levin, 2011; Tamura et al., 2018). Observation records from Lingshui City show that the maximum monthly wind speed could reach 15 m/s to 28 m/s in the storm seasons (Zhou et al., 2019), suggesting that strong onshore winds associated with storms have the potential for transporting coarse grain deposits onshore in the southeastern Hainan Island.

However, some storms may be dominated by offshore winds (Nott et al., 2013), which have no possibility of transporting coarse particles onshore. In addition, precipitation associated with storms may wet the beaches, reducing the possibility of coarse sand being transported onshore. In the front dune of the JL site, huge thick storm deposits (5-7 m) with numerous current-generated horizontal planar bedding developed in the upper part of the JL-A and JL-B profiles over the past 300 years (Figures 3B, 6). Similarly, storm deposits with numerous current-generated horizontal planar bedding were also identified in the LA-E profile and other profiles on the LA site (Zhou et al., 2019a) over the past 3000 years. This means that the repeated storm wave runup should be the primary process responsible for transporting the coarse-sand fractions at least in the JL-A site and LA-E site. However, the coarse sand deposits on the top of the LA dune field are >20 m asl, which means that storm wave run-up and currents both found it hard to reach this position. It is possible that part of the coarse sand fractions in the dune at the LA site were from the contribution of storm winds. Therefore, we have reason to think that storm wave runup and storm wind processes play a significant role in building the sand dunes in southeastern Hainan Island, as indicated by Tamura et al. (2018), especially sand dunes beyond the reach of fair-weather swash limit.

5 Conclusions

This paper aims to examine periods of dune development on southeastern Hainan Island using OSL dating data. The OSL ages result in this study have shown at least three periods of coastal sand accumulation: >28-21 ka BP, 14-4 ka BP, and 3.0 ka -present, which occurred during the LGM, late Pleistocene/early-mid Holocene, and late Holocene period. The first dune development in the P1 period (28-21 ka BP) was due to the extremely dry and cold weather and significant sea-level drop during the LGM period. The dune development in the P2 period (14-4 ka BP) is mainly associated with the relatively stronger winter monsoon. The strengthening of the winter monsoon due to climatic deterioration played an important role in the formation of the dune in the P3 period (3.0 ka-present). In addition, the grain size data analysis indicated that storm wave runup and storm wind processes also play a significant role in building the sand dunes in southeastern Hainan Island, especially the dunes beyond the reach of the fair-weather swash. This study further supported that coastal dunes have great potential in responding to paleoclimate changes, sea level rise, and storm activities. However, it remains to be worked out as to what extent storminess has controlled the dune formation in future work.

Data availability statement

The original contributions presented in the study are included in the article/Supplementary Material. Further inquiries can be directed to the corresponding authors.

Ethics statement

Written informed consent was obtained from the individual(s) for the publication of any potentially identifiable images or data included in this article.

Author contributions

LZ designed the research, analyzed the data, and wrote the manuscript. YY and GL wrote and revised parts of manuscript. CT helped to revise the manuscript and the result analyses. All authors contributed to the article and approved the submitted version.

Acknowledgments

This study was supported by grants from the Natural Science Foundation of China (41530962; 41706096); Opening Foundation of Hainan Key Laboratory of Marine Geological Resources and Environment (HNHYDZZYHJKF005; HNHYDZZYHJKF015); Hainan Provincial Natural Science Foundation of China (422RC800). We thank Baoming Yang, Jiayu Tu, Longhui Zhang, Chen Dai, and Danan Wang for their help with fieldwork, and Pro. Yaping Wang, Pro. Jianhua Gao, Pro. Peihong Jia for technical support.

Conflict of interest

The authors declare that the research was conducted in the absence of any commercial or financial relationships that could be construed as a potential conflict of interest.

Publisher's note

All claims expressed in this article are solely those of the authors and do not necessarily represent those of their affiliated organizations, or those of the publisher, the editors and the reviewers. Any product that may be evaluated in this article, or claim that may be made by its manufacturer, is not guaranteed or endorsed by the publisher.

Supplementary material

The Supplementary Material for this article can be found online at: https://www.frontiersin.org/articles/10.3389/fmars.2023.1165551/full#supplementary-material

References

Aagaard, T., Orford, J., and Murray, A. S. (2007). Environmental controls on coastal dune formation; skallingen spit, Denmark. *Geomorphology* 83 (1-2), 29–47. doi: 10.1016/j.geomorph.2006.06.007

Adamiec, G., and Aitken, M. J. (1998). Doserate conversion factors: update. *Ancient TL* 16 (2), 37–50.

Alappat, L., Seralathan, P., Shukla, A. D., Thrivikramji, K. P., and Singhvi, A. K. (2013). Chronology of red dune aggradations of south India and its palaeo-environmental significance. *Geochronometria* 40, 274–282. doi: 10.2478/s13386-013-0118-5

Arnold, L. J., Bailey, R. M., and Tucker, G. E. (2007). Statistical treatment of fluvial dose distributions from southern colorado arroyo deposits. *Quat. Geochronol.* 2 (1), 162–167. doi: 10.1016/j.quageo.2006.05.003

Ashkenazy, Y., Yizhaq, H., and Tsoar, H. (2012). Sand dune mobility under climate change in the Kalahari and Australian deserts. *Climatic. Change.* 112 (3), 901–923. doi: 10.1007/s10584-011-0264-9

Bardají, T., Goy, J. L., Zazo, C., Hillaire-Marcel, C., Dabrio, C. J., Cabero, A., et al. (2009). Sea Level and climate changes during OIS5e in the Western Mediterranean. *Geomorphology* 104 (1-2), 22–37. doi: 10.1016/j.geomorph.2008.05.027

Blott, S. J., and Pye, K. (2001). GRADISTAT: a grain size distribution and statistics package for the analysis of unconsolidated sediments. *Earth. Surf. Proc. Land.* 26 (11), 1237–1248. doi: 10.1002/esp.261

Chamberlain, E. L., Wallinga, J., Reimann, T., Goodbred, S. L.Jr., Steckler, M. S., Shen, Z., et al. (2017). Luminescence dating of delta sediments: novel approaches explored for the Ganges-Brahmaputra-Meghna delta. *Quaternary Geochronol.* 41, 97–111. doi: 10.1016/j.quageo.2017.06.006

Chazan, M., Porat, N., Sumner, T. A., and Horwitz, L. K. (2013). The use of OSL dating in unstructured sands: the archaeology and chronology of the hutton sands at canteen kopje (Northern cape province, south Africa). *Archaeol. Anthrop. Sci.* 5, 351–363. doi: 10.1007/s12520-013-0118-7

Clemmensen, L. B., Hansen, K. W., and Kroon, A. (2014). Storminess variation at skagen, northern Denmark since AD 1860: relations to climate change and implications for coastal dunes. *Aeolian. Res.* 15, 101–112. doi: 10.1016/j.aeolia.2014.09.001

Clemmensen, L. B., Murray, A. S., and Nielsen, L. (2012). Quantitative constraints on the sea-level fall that terminated the littorina Sea stage, southern Scandinavia. *Quaternary Sci. Rev.* 40, 54–63. doi: 10.2478/s13386-011-0048-z

Colin, V. M., Jones, B. G., Tran, N., Price, D. M., Vinh, V. V., Tinh, T. N., et al. (2002). Thermoluminescence ages for a reworked coastal barrier, southeastern Vietnam: a preliminary report. *J. Asian. Earth. Sci.* 20 (5), 535–548. doi: 10.1016/S1367-9120(01)00040-2

Cunningham, A. C., Wallinga, J., and Minderhoud, P. S. (2011). Expectations of scatter in equivalent-dose distributions when using multi-grain aliquots for OSL dating. *Geochronometria* 38, 424–431. doi: 10.2478/s13386-011-0048-z

Defeo, O., McLachlan, A., Schoeman, D. S., Schlacher, T. A., Dugan, J., Jones, A., et al. (2009). Threats to sandy beach ecosystems: a review. *Estuar. Coast. Shelf.* S. 81 (1), 1–12. doi: 10.1016/j.ecss.2008.09.022

Dissanayake, P. M. P. K., Brown, J., and Karunarathna, H. (2015). Impacts of storm chronology on the morphological changes of the formby beach and dune system, UK. *Nat. Hazard Earth. Sys.* 15 (7), 1533–1543. doi: 10.5194/nhess-15-1533-2015

Fu, X., Liu, Y., Wang, M., Peng, X., Fu, Y., Shou, J., et al. (2016). Neolithic remains in southeastern coastal areas of hainan. *Archaelogy* 7), 723–738.

Galbraith, R. F., Roberts, R. G., Laslett, G. M., Yoshida, H., and Olley, J. M. (1999). Optical dating of single and multiple grains of quartz from jinmium rock shelter, northern Australia: part I, experimental design and statistical models. *Archaeometry* 41 (2), 339–364. doi: 10.1111/j.1475-4754.1999.tb00987.x

Gao, L., Long, H., Zhang, P., Tamura, T., Feng, W., and Mei, Q. (2019). The sedimentary evolution of Yangtze river delta since MIS3: a new chronology evidence revealed by OSL dating. *Quat. Geochronol.* 49, 153–158. doi: 10.1016/j.quageo.2018.03.010

Grün, R. (2009). The DATA program for the calculation of ESR age estimates on tooth enamel. *Quat. Geochronol.* 4 (3), 231–232. doi: 10.1016/j.quageo.2008.12.005

Guo, Y., Ge, Y., Mao, P., and Liu, T. (2023). A comprehensive analysis of Holocene extraordinary flood events in the langxian gorge of the yarlung tsangpo river valley. *Sci. Total Environ.* 863, 160942. doi: 10.1016/j.scitotenv.2022.160942

Harris, M. E., and Ellis, J. T. (2021). Comparing tropical cyclone and king tide impacts on a south Carolina coastal dune system. *J. Coastal. Res.* 37 (5), 923–932. doi: 10.2112/JCOASTRES-D-21-00025.1

Hu, F., Li, Y., Liang, J., Li, Z., Xie, M., Chen, X., et al. (2022). History of coastal dune evolution in the fujian region of southeastern China over the last millenium. *Mar. Geol.* 451, 106878. doi: 10.1016/j.margeo.2022.106878

Jiang, T., Liu, X., Yu, T., and Hu, Y. (2018). OSL dating of late Holocene coastal sediments and its implication for sea-level eustacy in hainan island, southern China. *Quat. Int.* 468, 24–32. doi: 10.1016/j.quaint.2017.11.039

Jin, J., Ling, Z., Li, Z., Zuo, X., Fan, X., Huang, Y., et al. (2022). Spatiotemporal distribution of sea-island prehistoric dune sites, Holocene sea levels, and aeolian sand activities in fujian province, China. *J. Geogr. Sci.* 32 (6), 1157–1176. doi: 10.1007/s11442-022-1990-9

Kunz, A., Frechen, M., Ramesh, R., and Urban, B. (2010). Luminescence dating of late Holocene dunes showing remnants of early settlement in cuddalore and evidence of monsoon activity in south east India. *Quat. Int.* 222 (1-2), 194–208. doi: 10.1016/j.quaint.2009.10.042

Lang, A., Lindauer, S., Kuhn, R., and Wagner, G. A. (1996). Procedures used for optically and infrared stimulated luminescence dating of sediments in Heidelberg. *Ancient TL* 14 (3), 7–11.

Levin, N. (2011). Climate-driven changes in tropical cyclone intensity shape dune activity on earth's largest sand island. *Geomorphology* 125 (1), 239–252. doi: 10.1016/j.geomorph.2010.09.021

Li, S., Liu, X., Li, H., Zheng, Y., and Wei, X. (2007). A wind tunnel simulation of the dynamic processes involved in sand dune formation on the western coast of hainan island. *J. Geogr. Sci.* 17, 453–468. doi: 10.1007/s11442-007-0453-7

Martinez, M. L., Silva, R., Mendoza, E., Odériz, I., and Pérez-Maqueo, O. (2016). Coastal dunes and plants: an ecosystem-based alternative to reduce dune face erosion. *J. Coastal. Res.* 75 (10075), 303–307. doi: 10.1016/j.ecss.2019.01.018

Maximiliano-Cordova, C., Martínez, M. L., Silva, R., Hesp, P. A., Guevara, R., and Landgrave, R. (2021). Assessing the impact of a winter storm on the beach and dune systems and erosion mitigation by plants. *Front. Mar. Sci.* 8. doi: 10.3389/fmars.2021.734036

Mertens, K. N. J. M., Lynn, M., Aycard, M., Lin, H.-L., and Louwye, S. (2009). Coccolithophores as palaeoecological indicators for shifts of the ITCZ in the cariaco basin during the late quaternary. *J. Quat. Sci.* 24 (2), 159–174. doi: 10.1002/jqs.1194

Morris, R. L., Boxshall, A., and Swearer, S. E. (2020). Climate-resilient coasts require diverse defence solutions. *Nat. Clim. Change.* 10 (6), 485–487. doi: 10.1038/s41558-020-0798-9

Murray, A. S., and Clemmensen, L. B. (2001). Luminescence dating of Holocene aeolian sand movement, thy, Denmark. *Quaternary Sci. Rev.* 20 (5-9), 751–754. doi: 10.1016/S0277-3791(00)00061-5

Murray, A. S., and Wintle, A. G. (2003). The single aliquot regenerative dose protocol: potential for improvements in reliability. *Radiat. Measurements* 37 (4-5), 377–381. doi: 10.1016/S1350-4487(03)00053-2

Murray-Wallace, C. V., Bourman, R. P., Prescott, J. R., Williams, F., Price, D. M., and Belperio, A. P. (2010). Aminostratigraphy and thermoluminescence dating of coastal aeolianites and the later quaternary history of a failed delta: the river Murray mouth region, south Australia. *Quat. Geochronol.* 5 (1), 28–49. doi: 10.1016/j.quageo.2009.09.011

Nian, X., Zhang, W., Wang, Z., Sun, Q., and Chen, Z. (2021). Inter-comparison of optically stimulated luminescence (OSL) ages between different fractions of Holocene deposits from the Yangtze delta and its environmental implications. *Mar. Geol.* 432, 106401. doi: 10.1016/j.margeo.2020.106401

Nott, J., Chague-Goff, C., Goff, J., Sloss, ,. C., and Riggs, ,. N. (2013). Anatomy of sand beach ridges: evidence from severe tropical cyclone yasi and its predecessors, northeast Queensland, australia. J. *Geophys. Res. Earth Surf.* 118, 1710– 1719. doi: 10.1002/jgrf.20122

Reimann, T., Lindhorst, S., Thomsen, K. J., Murray, A. S., and Frechen, M. (2012). OSL dating of mixed coastal sediment (Sylt, German bight, north Sea). *Quat. Geochronol.* 11, 52–67. doi: 10.1016/j.quageo.2012.04.006

Robin, N., Billy, J., Castelle, B., Hesp, P., Lerma, A. N., Laporte-Fauret, Q., et al. (2021). 150 years of foredune initiation and evolution driven by human and natural processes. *Geomorphology* 374, 107516. doi: 10.1016/j.geomorph.2020.107516

Searle, D. J., and Woods, P. J. (1986). Detailed documentation of a Holocene sea-level record in the Perth region, southern Western Australia. *Quat. Res.* 26 (3), 299–308. doi: 10.1016/0033-5894(86)90091-8

Sommerville, A. A., Hansom, J. D., Sanderson, D. C. W., and Housley, R. A. (2003). Optically stimulated luminescence dating of large storm events in northern Scotland. *Quaternary Sci. Rev.* 22 (10-13), 1085–1092. doi: 10.1016/S0277-3791(03)00057-X

Song, C. (1984). Geomorphology and the tidal inlets in the East coast of hainan island. *Studia Mar. Sci. South China Sea (in Chinese)* 5), 31–50.

Steinke, S., Glatz, C., Mohtadi, M., Groeneveld, J., Li, Q., and Jian, Z. (2011). Past dynamics of the East Asian monsoon: no inverse behaviour between the summer and winter monsoon during the Holocene. *Global Planet. Change.* 78 (3-4), 170–177. doi: 10.1016/j.gloplacha.2011.06.006

Tamura, T., Bateman, M. D., Kodama, Y., Saitoh, Y., Watanabe, K., Yamaguchi, N., et al. (2011a). Building of shore-oblique transverse dune ridges revealed by ground-penetrating radar and optical dating over the last 500 years on tottori coast, Japan Sea. *Geomorphology* 132 (3-4), 153–166. doi: 10.1016/j.geomorph.2011.05.005

Tamura, T., Kodama, Y., Bateman, M. D., Saitoh, Y., Watanabe, K., Matsumoto, D., et al. (2011b). Coastal barrier dune construction during sea-level highstands in MIS 3 and 5a on tottori coast-line, Japan. *Palaeogeogr. Palaeocl.* 308 (3-4), 492–501. doi: 10.1016/j.palaeo.2011.05.054

Tamura, T., Kodama, Y., Bateman, M. D., Saitoh, Y., Yamaguchi, N., and Matsumoto, D. (2016). Late Holocene aeolian sedimentation in the tottori coastal dune field, Japan Sea, affected by the East Asian winter monsoon. *Quat. Int.* 397, 147–158. doi: 10.1016/j.quaint.2015.09.062

Tamura, T., Nicholas, W. A., Oliver, T. S., and Brooke, B. P. (2018). Coarse-sand beach ridges at Cowley beach, north-eastern Australia: their formative processes and potential as records of tropical cyclone history. *Sedimentology.* 65 (3), 721–744. doi: 10.1111/sed.12402

Tamura, T., Ta, T. K. O., Saito, Y., Bateman, M. D., Murray-Wallace, C. V., Nguyen, T. M. L., et al. (2020). Seasonal control on coastal dune morphostratigraphy under a monsoon climate, mui Ne dunefield, SE Vietnam. *Geomorphology* 370, 107371. doi: 10.1016/j.geomorph.2020.107371

van Heteren, S., Huntley, D. J., van de Plassche, O., and Lubberts, R. K. (2000). Optical dating of dune sand for the study of sea-level change. *Geology* 28 (5), 411–414. doi: 10.1130/0091-7613(2000)28%3C411:ODODSF%3E2.0.CO;2

Waelbroeck, C., Labeyrie, L., Michel, E., Duplessy, J. C., McManus, J. F., Lambeck, K., et al. (2002). Sea-Level and deep water temperature changes derived from benthic foraminifera isotopic records. *Quat. Sci. Rev.* 21 (1–3), 295–305. doi: 10.1016/S0277-3791(01)00101-9

Wang, W. (1997). The formation and paleogeographical environment of old red sand in south China. *Sci. China: Ser. D* 27 (6), 537–542.

Wang, Y., Peter, M. I., Zhu, D., Zhang, Y., and Tang, W. (2001). Coastal plain evolution in southern hainan island, China. *Chinese. Sci. Bull.* 46 (1), 90–96. doi: 10.1007/BF03187244

Wang, D., Wang, Y. P., Yang, Y., Gao, J., and Yang, Y. (2016). The characteristics and mechanism of suspended sediment transport in lagoon: a case study from xincun and LiAn harbors, hainan island. *Quat Sci.* 36 (1), 154–162. doi: 10.11928/ j.issn.1001-7410.2016.15

Wolfe, S., Bond, J., and Lamothe, M. (2011). Dune stabilization in central and southern Yukon in relation to early Holocene environmental change, northwestern north America. *Quaternary Sci. Rev.* 30 (3-4), 324–334. doi: 10.1016/j.quascirev.2010.11.010

Wu, Z., and Wang, W. (1997). The formation and paleogeographical environment of old red sand in South China. . *Sci. China Ser. B.* 27 (6), 537–548 (In Chinese with English Abstract).

Wu, Z., and Wu, K. Z. (1995). Holocene Coastal dune along the south China coast. *Sci. China Ser. B.* 25 (2), 211–218.

Xu, F., Hu, B., Dou, Y., Song, Z., Liu, X., Yuan, S., et al. (2018). Prehistoric heavy metal pollution on the continental shelf off hainan island, south China Sea: from natural to anthropogenic impacts around 4.0 kyr BP. *Holocene* 28 (3), 455–463. doi: 10.1177/09596836177294

Yamamoto, M., Sai, H., Chen, M. T., and Zhao, M. (2013). The East Asian winter monsoon variability in response to precession during the past 150 000 yr. *Clim. Past.* 9 (6), 2777–2788. doi: 10.5194/cp-9-2777-2013

Zazo, C., Dabrio, C. J., Goy, J. L., Lario, J., Cabero, A., Silva, P. G., et al. (2008). The coastal archives of the last 15 ka in the Atlantic–Mediterranean Spanish linkage area: Sea level and climate changes. *Quat. Int.* 181 (1), 72–87. doi: 10.1016/j.quaint.2007.05.021

Zhang, Y., Huang, C. C., Shulmeister, J., Guo, Y., Liu, T., Kemp, J., et al. (2019). Formation and evolution of the Holocene massive landslide-dammed lakes in the jishixia gorges along the upper yellow river: no relation to china's great flood and the xia dynasty. *Quaternary Sci. Rev.* 218, 267–280. doi: 10.1016/j.quascirev.2019.06.011

Zhang, J. F., Liu, C. L., Wu, X. H., Liu, K. X., and Zhou, L. P. (2012). Optically stimulated luminescence and radiocarbon dating of sediments from lop nur (Lop nor), China. *Quaternary Geochronol.* 10, 150–155. doi: 10.1016/j.quageo.2011.12.001

Zhao, Y., Yu, Z., Chen, F., Zhang, J., and Yang, B. (2009). Vegetation response to Holocene climate change in monsoon-influenced region of China. *Earth-Science Rev.* 97 (1-4), 242–256. doi: 10.1016/j.earscirev.2009.10.007

Zheng, S., Cheng, H., Lv, J., Li, Z., and Zhou, L. (2021). Morphological evolution of estuarine channels influenced by multiple anthropogenic stresses: A case study of the north channel, Yangtze estuary, China. *Estuar. Coast. Shelf S.* 249, 107075. doi: 10.1016/j.ecss.2020.107075

Zhou, L., Gao, S., Jia, J., Zhang, Y., Yang, Y., Mao, L., et al. (2019a). Extracting historic cyclone data from coastal dune deposits in eastern hainan island, China. *Sediment. Geol.* 392, 105524. doi: 10.1016/j.sedgeo.2019.105524

Zhou, L., Yang, Y., Wang, Z., Jia, J., Mao, L., Li, Z., et al. (2019b). Investigating ENSO and WPWP modulated typhoon variability in the south China Sea during the mid–late Holocene using sedimentological evidence from southeastern hainan island, China. *Mar. Geol.* 416, 105987. doi: 10.1016/j.margeo.2019.105987